

Video Article

Using Optical Coherence Tomography and Optokinetic Response As Structural and Functional Visual System Readouts in Mice and Rats

Michael Dietrich¹, Christina Hecker¹, Alexander Hilla², Andrés Cruz-Herranz³, Hans-Peter Hartung¹, Dietmar Fischer², Ari Green³, Philipp Albrecht¹

¹Department of Neurology, Heinrich-Heine-University Düsseldorf

²Department of Cell Physiology, Faculty of Biology and Biotechnology, Ruhr-University Bochum

³Division of Neuroinflammation and Glial Biology, Department of Neurology, University of California San Francisco

Correspondence to: Philipp Albrecht at phil.albrecht@gmail.com

URL: <https://www.jove.com/video/58571>

DOI: [doi:10.3791/58571](https://doi.org/10.3791/58571)

Keywords: Optical coherence tomography, optokinetic response, ocular imaging, visual pathway, holder, rodent models

Date Published: 12/13/2018

Citation: Dietrich, M., Hecker, C., Hilla, A., Cruz-Herranz, A., Hartung, H.P., Fischer, D., Green, A., Albrecht, P. Using Optical Coherence Tomography and Optokinetic Response As Structural and Functional Visual System Readouts in Mice and Rats. *J. Vis. Exp.* (), e58571, doi:10.3791/58571 (2018).

Abstract

Optical coherence tomography (OCT) is a fast, non-invasive, interferometric technique allowing high-resolution retinal imaging. It is an ideal tool for the investigation of processes of neurodegeneration, neuroprotection and neuro-repair involving the visual system, as these often correlate well with retinal changes. As a functional readout, visually evoked compensatory eye and head movements are commonly used in experimental models involving the visual function. Combining both techniques allows a quantitative *in vivo* investigation of structure and function, which can be used to investigate the pathological conditions or to evaluate the potential of novel therapeutics. A great benefit of the presented techniques is the possibility to perform longitudinal analyses allowing the investigation of dynamic processes, reducing variability and cuts down the number of animals needed for the experiments. The protocol described aims to provide a manual for acquisition and analysis of high quality retinal scans of mice and rats using a low cost customized holder with an option to deliver inhalational anesthesia. Additionally, the proposed guide is intended as an instructional manual for researchers using optokinetic response (OKR) analysis in rodents, which can be adapted to their specific needs and interests.

Video Link

The video component of this article can be found at <https://www.jove.com/video/58571/>

Introduction

The examination of the visual pathway, as a part of the central nervous system, has been proven to be an effective starting point in addressing not only ophthalmologic^{1,2,3,4,5}, but also neurologic^{6,7,8,9,10,11,12,13,14,15,16} questions. In recent years, OCT and OKR have been identified as useful analytic, non-invasive tools to evaluate a large variety of retinopathies and retinal manifestations in various rodent models^{17,18,19,20,21,22,23,24,25}. OCT allows for fast and high resolution *in vivo* visualization of the retinal morphology and structure in mice and rats, with results in good accordance with histological sections of the animals retinae²⁶. OKR constitutes a fast and robust method to quantitatively assess visual function.

Many OCT devices allow simultaneous confocal scanning laser ophthalmoscopy (cSLO) imaging with different wavelengths, which provides diagnostic information about retinal pathologies, i.e., visualization of lipofuscin deposits or alterations of the retinal pigment epithelium²⁷. Furthermore, *in vivo* imaging of fluorescence labelled cells in transgenic animals is possible^{28,29,30,31,32}. However, the application of OCT technology in rodent models is still challenging, mainly because of the small eye size. Several commercially available devices require adaptations and often a different size of holder is required to image the animals of different species. Additionally, animals require anesthesia for measurement.

OKR devices can be used to assess the visual function in rodents. The animals are placed on a platform in the center of an actual or virtual cylinder displaying a moving grating, which the animals track with reflexive head and neck movements. This optokinetic response is reduced or eliminated in the case of the reduction or loss of visual function.

The aim of this protocol is to present a manual for the measurement of retinal thickness using a commercially available OCT device with a custom holder providing inhalant anesthesia. The protocol illustrates how to analyze volume scans using the software provided by the manufacturer. For visual testing, the aim is to provide instructions on how to use a commercially available system to assess the OKR.

Protocol

All animal procedures were performed in compliance with the experimental guidelines approved by the regional authorities (State Agency for Nature, Environment and Consumer Protection) and conform to the Association for Research in Vision and Ophthalmology (ARVO) Statement for the Use of Animals in Ophthalmic and Vision Research.

1. Confocal Scanning Laser Ophthalmoscopy-optical Coherence Tomography

NOTE: The protocol for cSLO-OCT measurement is adaptable for all strains of laboratory mice and rats.

1. Set-up and pre-imaging preparations

NOTE: The system configuration of the OCT device used in this protocol has already been described elsewhere³¹.

2. Rodent preparation for inhalant anesthesia

1. Place the rodent in an induction chamber and set the vaporizer to an isoflurane concentration of 2% at 2 L/min O₂.
2. Check if the rodent is anesthetized by pinching the tail, remove it from the chamber and wrap it in paper towel to keep it warm.
3. Place the rodent in the custom holder³³ and hook the maxillary incisors on the integrated bite bar of the mouth piece, connected to the vaporizer (2.5% isoflurane at 2 L/min O₂).
4. Apply one drop of Phenylephrine 2.5%-Tropicamide 0.5% on each eye for pupillary dilation.
5. Wipe off any excess liquid of eye drops after 1 min and lubricate the eyes with methyl-cellulose based ophthalmic gel (e.g., hypromellose 0.3% eye drops) to avoid drying out and turbidity of the cornea.
6. Place custom contact lens (+4 diopters) on the mouse eye by hand or using forceps. Cover the rat eye with a glass plate (e.g., round 12 mm diameter glass coverslip) without optical properties to assure a plane surface.

3. Measurement and analysis

NOTE: Make sure to perform and report the OCT measurements in line with the APOSTEL recommendations³⁴ and perform quality control according to the OSCAR-IB consensus criteria³⁵. As these recommendations have been developed for human OCT images, some criteria are not or only partially applicable.

1. To image the right eye, position the holder as presented in **Figure 1A** to ensure that the right eye bulb of the rodent faces the camera.
2. Press the **Start** button in the right corner of the control panel display to start the acquisition mode.
3. Set the filter lever to **R** and select **BR+OCT for Blue reflectance** fundus imaging and B-scan acquisition on the control panel.
4. Set the focus distance to approx. 38 diopters using the focus knob on the back of the camera and zoom in on the retina until the OCT scan is visible on the screen.
NOTE: At the first measurement, the reference arm has to be adapted for rodent measurement. Press the combination Ctrl+Alt+Shift +O and adjust the value of the reference arm in the open window until the OCT-scan appears on the screen.
5. To ensure a beam path through the middle of the pupil with an orthogonal angle to the retina in all planes, position the optic disc in the middle of the illuminated field (BR) and adjust the horizontal and vertical line B-scans to a horizontal level by rotating/turning the holder (**Figure 1B**) or moving the camera.
6. Select the volume scan mode and set it to 25 B-scans in high-resolution mode at 50 automatic real-time tracking (ART, rasterized from 50 averaged A-Scans) on the software screen.
7. Center the middle of the volume scan grid on the optic disc and start acquisition by pressing the black sensitivity knob and then **AQUIRE** on the control panel.
8. Set the filter lever to **A**, select **Blue Auto Florescence (BAF)** on the control panel and adjust image brightness with the sensitivity knob. Press the sensitivity knob and then **AQUIRE** to image fluorescent cells (e.g., EGFP) or auto fluorescent deposits.
9. Apply ophthalmic gel on the eye of the rodent to prevent dehydration and put the animal in a separate cage with a heat source.
10. Supervise the rodent until it is fully recovered from anesthesia. When the animal is ambulatory, return it to the home cage.
11. For analysis of the volume scans, use the automated segmentation of the OCT device's software by right-clicking on the scan and select **Segmentation** then **All Layers**. Make sure that the quality of the OCT images is sufficient and define quality cutoffs for each set of experiments, e.g., >20 decibels.
12. Perform manual correction of the layers by double clicking on the desired scan, select **Thickness Profile** and click on **Edit Layer Segmentations**. Select one layer, e.g., press ILM for **Inner limiting membrane**, and, if necessary, correct the green line by moving the red dots by drag and drop to the correct position.
NOTE: Make sure the investigator performing the manual correction is blinded for the experimental groups.
13. Select the tab **Thickness Map** and choose the **1, 2, 3 mm** early treatment of diabetic retinopathy study (ETDRS) grid. Center the inner circle on the optic disc (**Figure 2**, left).
14. Calculate the thickness of retinal layers from the thickness values provided by the software for the different retinal sectors of interest. To compute the mean thickness values from volume scans, use the whole 1, 2, 3 mm ETDRS grid, which covers an angle of approximately 25°, excluding the inner 1 mm circle, which contains the optic disc (**Figure 2**, right).
15. Perform the statistical analysis using adequate software. If both eyes of an animal are included, consider a statistical model accounting for within subject inter-eye correlations (e.g., generalized estimating equations or mixed linear models), as the eyes of one subject are statistically dependent³⁶.

2. Optokinetic Response

NOTE: In the following, a detailed manual for OKR measurements of mice and rats is provided, which can be adapted to individual specific needs.

1. Set-up and pre-measurement preparations

1. Turn on the computer. After the system has booted, turn on the screens of the testing chamber as described in more detail elsewhere³⁷.
2. Select a suitable platform for the measurement of mice or rats.
NOTE: The platform size is selected based on the body size of the rodent. The animal should be able to sit properly on the platform without the ability to walk around.
3. Open the pre-settings window by double-clicking on the software, select **New group** and choose the group name, the number of subjects, the species and strains. Select a variable stimulus: spatial/temporal frequency, contrast sensitivity, speed or orientation in the drop-down menu, then press **OK**.
4. Focus on the platform by manipulating the focus ring of the camera on top of the chamber and calibrate the system by aligning (drag and drop) the red circle around the black circle on the platform.

2. Measurement and analysis

1. Place the animal on the platform, let it adapt to the environment for ~5 min. Lift the animal back on platform if it drops (**Figure 3A**).
2. Select **Subject** number and **Condition** on the top right corner of the software screen (**Figure 3B**). One stimulus is variable, the other stimuli are kept constant. This is confirmed by the **Open lock** or **Closed lock** symbol next to the stimulus.
3. Start measurement by selecting ◀ for **Yes** or ■ for **No**, if the animal tracks or does not track, respectively.
NOTE: Clockwise tracking corresponds to the left and counterclockwise tracking to the right eye. The software randomly changes the direction of the moving grid.
4. Select the step size of the stimulus manually by clicking on the **Up** and **Down** arrows next to the variable stimulus or let it adapt automatically by the software if stimulus threshold converges.
5. For optimal results, animate the animal, e.g., by high whistling sounds and blanking, by clicking the black or white box symbol on the software screen. Perform these actions repeatedly in the case of prolonged measurements.
6. For data analysis, select the **Summary** tab and click on **File | Export Table/Graph** to export the desired data set.
7. Perform the statistical analysis using the desired software (see also Step 1.3.15).

Representative Results

Using 3rd generation OCT imaging in myelin oligodendrocyte glycoprotein (MOG) peptide induced experimental autoimmune encephalomyelitis (EAE) mouse models, high-resolution morphological sections of the mouse retina were obtained. Using this technology, the protective capacities of different substances were demonstrated¹⁷. The thickness values of the inner retinal layers (IRL) obtained are in good accordance with the numbers of retinal ganglion cells (RGC) obtained by histological staining of retinal wholemounts (**Figure 4**).

OKR monitoring provides a functional readout of the neurodegeneration seen by OCT. In these experiments, visual function assessed as spatial frequency by OKR, and neuroaxonal damage assessed as IRL thinning by OCT, were in close correlation¹⁷. Various protocols can be employed to examine the visual acuity by changing the spatial or temporal frequency, contrast sensitivity, orientation or speed of the moving grid. In the EAE model, an improved spatial frequency of 0.05 cycles/degree (c/d) of animals treated with substance 1 was detected compared to untreated MOG-EAE mice (**Figure 5**).

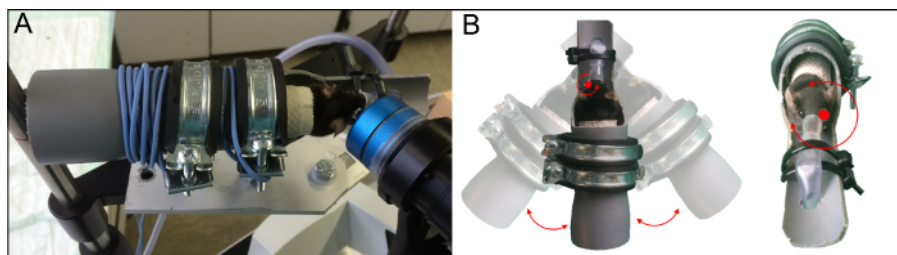


Figure 1: Custom holder for OCT measurement. (A) OCT imaging of a C57BL/6J mouse using the custom holder³³ and (B) rotational axis around the rodent eye. Rotation in the transverse plane (left) and in the axial plane (right) is demonstrated. This figure has been modified from Dietrich, M. et al.³³. [Please click here to view a larger version of this figure.](#)

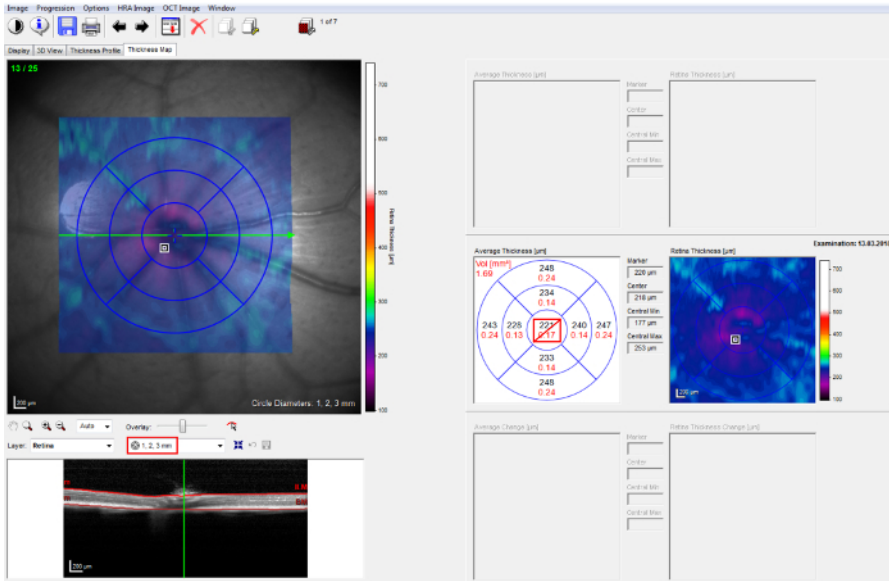


Figure 2: OCT post acquisition analysis. "1, 2, 3 mm" ETDRS grid on the 25 B-scan volume protocol (left). The thickness of retinal layers is provided for the different retinal sectors by the software (right). [Please click here to view a larger version of this figure.](#)

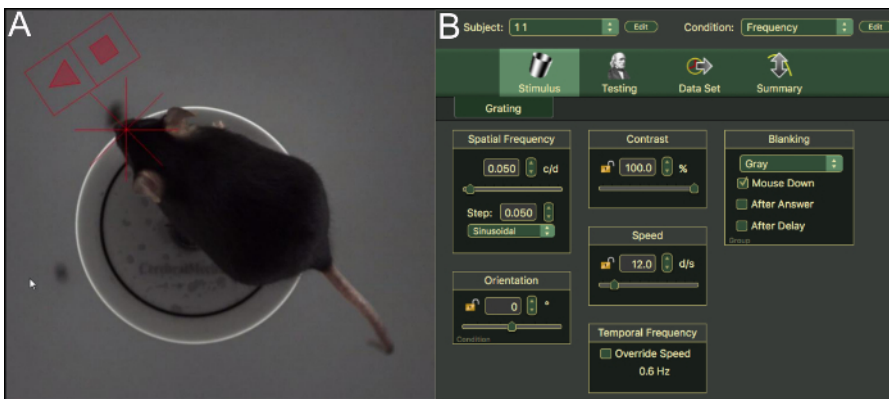


Figure 3: OKR measurement of mice and stimulus settings. (A) Top view through the camera analyzing a C57BL/6J mouse on the platform in the chamber. (B) User interface and settings of the OKR software. [Please click here to view a larger version of this figure.](#)

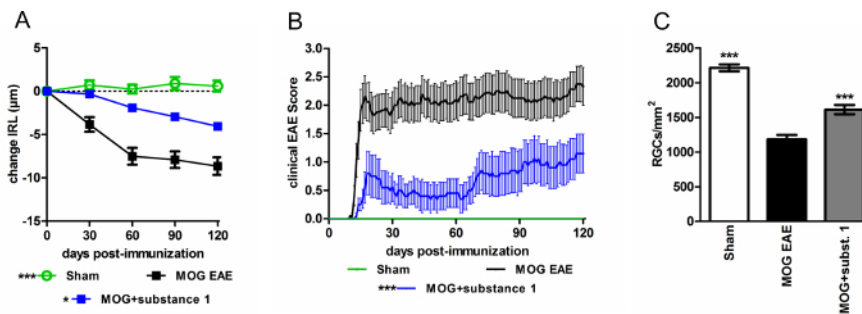


Figure 4: C57BL/6J mice with MOG EAE show an attenuated disease course when treated with substance 1 compared to untreated controls. (A) The degeneration of the inner retinal layers is reduced (B) and the clinical EAE score is attenuated during the EAE course when substance 1 was administered. Mice were scored daily, and OCT measurements were performed monthly over a period of 120 days. The graphs represent the mean and standard error of at least ten animals per group. ($*p < 0.05$, $***p < 0.001$, area under the curve compared by ANOVA with Dunnett's post hoc test). (C) The IRL thickness change is in good accordance with RGC loss ($***p < 0.001$, by ANOVA with Dunnett's post hoc test compared to MOG untreated mice). [Please click here to view a larger version of this figure.](#)

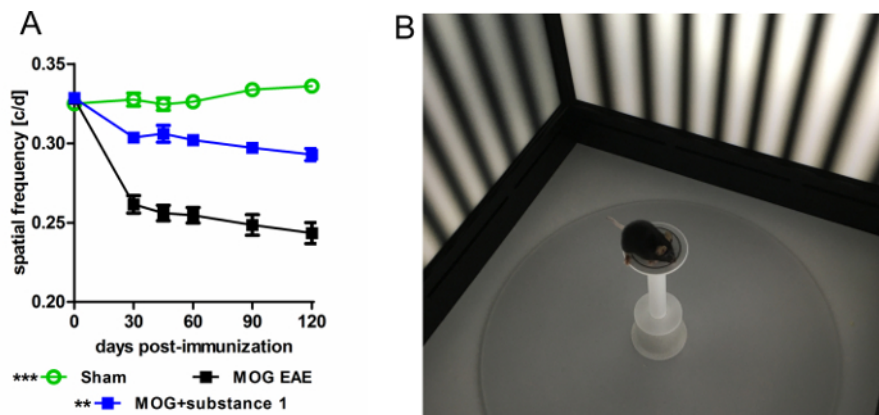


Figure 5: OKR measurement of C57BL/6J mice with MOG-EAE. (A) OKR reveals an improved visual acuity of animals treated with substance 1 compared to untreated MOG EAE mice measured by spatial frequency threshold testing over a period of 120 days. The graphs represent the mean and standard error of at least six animals per group (** $p < 0.01$, *** $p < 0.001$, area under the curve compared by ANOVA with Dunnett's post hoc test). **(B)** Image of a C57BL/6J mouse in the testing chamber. [Please click here to view a larger version of this figure.](#)

Discussion

This protocol provides an instruction for the thickness measurements and the examination of visual function in rodents. Visual readouts are increasingly used in translational research^{18,26,38,39,40} and are easily transferable to clinical trials. The significant advantage of OCT in comparison to histological investigations in animal experiments is that longitudinal analyses are possible allowing the investigation of dynamic pathological processes, largely reducing the variability and the number of animals needed per study. Furthermore, in vivo imaging with OCT is not subject to fixation, cutting or staining artifacts, which may affect the layer thickness in histological investigations.

However, the orthogonal orientation of the laser beam in all planes in relation to the retina is a critical step to ensure the quality and reproducibility of the thickness values. It requires some training of the investigator and is mandatory before the acquisition of OCT scans. Additionally, as the commercial devices are built for human applications, the quality of rodent OCT images is still inferior compared to B-scans of human patients. In the authors' experience, it may be difficult to distinguish the different inner retinal layers (retinal nerve fiber layer, ganglion cell layer and inner plexiform layer) during manual correction. We therefore recommend analyzing these layers as a compound readout (IRL).

The experimental setup provides an option for volatile anesthesia, e.g., inhalant isoflurane, which is, in our experience, safer and easier to control than injectable anesthesia, e.g., ketamine-xylazine^{41,42} and reduces the risk of premature awakening of rodents in case of longer acquisition times (e.g., when performing imaging of fluorescently labelled cells). In a preliminary study, volume scans were identified as the protocols with the highest validity and reliability. The inter-rater and test retest reliability was excellent when volume scans excluding the central part containing the optic disc were assessed with ICC (intra-class correlation coefficient) values above 0.85 for all assessments.

The measurement of the optokinetic response is based on the involuntary optokinetic reflex, which occurs in response to a continuously moving field. In rodents, in contrast to other species, the movement involves not only the eyes, but the whole head, which can easily be detected using the camera.

Distinguishing between "tracking" or normal behavioral movements of the animals requires some training of the investigator and it is important to be blinded for the experimental group. In addition, the animals need an adaption phase to accommodate to the experimental setting and during long-time measurement protocols, the animals have to be animated repeatedly to assure that "no tracking" is due to reaching the OKR threshold and not to decreasing attention. There is also a significant strain variability regarding the visual function of laboratory mice and rats^{43,44}. The visual acuity of the rodent should therefore be evaluated before they are tested and some strains, such as SJL mice, may not even be suitable for OKR measurements, as they are homozygous for the allele *Pde6brd1* (retinal degeneration 1).

In summary, the examination of retinal morphology and visual function in animal models allows for non-invasive, longitudinal investigations of structural and functional damage occurring in the context of EAE and may be helpful in other models involving the visual system, including but not limited to the models of retinopathies or optic nerve injury.

Disclosures

Unrelated to the work presented the authors declare the following financial disclosures:

Michael Dietrich received speaker honoraria from Novartis. Andrés Cruz-Herranz is a postdoctoral fellow of the National Multiple Sclerosis Society. Ari J. Green served on the scientific advisory board of MedImmune, Novartis, OCTIMS, Inception 5 Biosciences, and Bionure; is an associate editor of JAMA Neurology; was an editorial board member of Neurology; holds a patent for remyelination molecules and pathways; consulted for Inception 5 Sciences; received research support from Novartis Pharma OCTIMS, Inception Sciences SRA, NINDS, NIA, National MS Society, Sherak Foundation, and Hilton Foundation; holds stock or stock options in Inception 5; and served as an expert witness at Mylan v Teva Pharma. Hans-Peter Hartung has received fees for serving on steering committees from Biogen Idec, GeNeuro, Sanofi Genzyme, Merck, Novartis Pharmaceuticals, Octapharma, Opexa Therapeutics, Teva Pharmaceuticals, MedImmune, Bayer HealthCare, Forward Pharma, and Roche, fees for serving on advisory boards from Biogen Idec, Sanofi Genzyme, Merck, Novartis Pharmaceuticals, Octapharma, Opexa

Therapeutics, Teva Pharmaceuticals, and Roche, and lecture fees from Biogen Idec, Sanofi Genzyme, Merck, Novartis Pharmaceuticals, Octapharma, Opexa Therapeutics, Teva Pharmaceuticals, MedImmune, and Roche. Philipp Albrecht received compensation for serving on Scientific Advisory Boards for Ipsen, Novartis, Biogen; he received speaker honoraria and travel support from Novartis, Teva, Biogen, Merz Pharmaceuticals, Ipsen, Allergan, Bayer Healthcare, Esai, UCB and Glaxo Smith Kline; he received research support from Novartis, Biogen, Teva, Merz Pharmaceuticals, Ipsen, and Roche. The other authors report no disclosures.

Acknowledgements

This work was supported by grants of the Dr. Robert Pflieger-Foundation and the IIselore Luckow-Foundation, as well as Biogen and Novartis to PA. Figure 1B was reproduced from "Whole-body positional manipulators for ocular imaging of anaesthetized mice and rats: A do-it-yourself guide. Dietrich, M., Cruz-Herranz, A., Yiu, H., Aktas, O., Brandt, A. U., Hartung, HP., Green, A., Albrecht, P. *BMJ Open Ophthalmology*. 1 (1), e000008, 2017" with permission from BMJ Publishing Group Ltd.

References

1. Folgar, F.A., Jaffe, G.J., Ying, G.-S., Maguire, M.G., Toth, C.A. Comparison of optical coherence tomography assessments in the comparison of age-related macular degeneration treatments trials. *Ophthalmology*. **121** (10), 1956-1965, (2014).
2. Mowatt, G. *et al.* Optical coherence tomography for the diagnosis, monitoring and guiding of treatment for neovascular age-related macular degeneration: a systematic review and economic evaluation. *Health Technology Assessment*. **18** (69), 1-254, (2014).
3. Schlanitz, F.G. *et al.* Identification of Drusen Characteristics in Age-Related Macular Degeneration by Polarization-Sensitive Optical Coherence Tomography. *American Journal of Ophthalmology*. **160** (2), 335-344.e1, (2015).
4. Makiyama, Y. *et al.* Prevalence and spatial distribution of cystoid spaces in retinitis pigmentosa: investigation with spectral domain optical coherence tomography. *Retina*. **34** (5), 981-988, (2014).
5. Al Rashaed, S., Khan, A.O., Nowilaty, S.R., Edward, D.P., Kozak, I. Spectral-domain optical coherence tomography reveals prelaminar membranes in optic nerve head pallor in eyes with retinitis pigmentosa. *Graefes' Archive for Clinical and Experimental Ophthalmology*. **22**, (2015).
6. Albrecht, P. *et al.* Retinal pathology in idiopathic moyamoya angiopathy detected by optical coherence tomography. *Neurology*. **85** (6), 521-527, (2015).
7. Albrecht, P., Fröhlich, R., Hartung, H.-P., Kieseier, B.C., Methner, A. Optical coherence tomography measures axonal loss in multiple sclerosis independently of optic neuritis. *Journal of Neurology*. **254** (11), 1595-1596, (2007).
8. Albrecht, P. *et al.* Retinal neurodegeneration in Wilson's disease revealed by spectral domain optical coherence tomography. *PLoS One*. **7** (11), e49825, (2012).
9. Albrecht, P. *et al.* Optical coherence tomography in parkinsonian syndromes. *PLoS One*. **7** (4), e34891, (2012).
10. Albrecht, P. *et al.* Degeneration of retinal layers in multiple sclerosis subtypes quantified by optical coherence tomography. *Multiple Sclerosis Journal*. **18** (10), 1422-1429, (2012).
11. Bhaduri, B. *et al.* Detection of retinal blood vessel changes in multiple sclerosis with optical coherence tomography. *Biomedical Optics Express*. **7** (6), 2321-2330, (2016).
12. Knier, B. *et al.* Optical coherence tomography indicates disease activity prior to clinical onset of central nervous system demyelination. *Multiple Sclerosis Journal*. **22** (7), 893-900, (2016).
13. Ringelstein, M. *et al.* Subtle retinal pathology in amyotrophic lateral sclerosis. *Annals of Clinical and Translational Neurology*. **1** (4), 290-297, (2014).
14. Ringelstein, M. *et al.* Retinal pathology in Susac syndrome detected by spectral-domain optical coherence tomography. *Neurology*. **85** (7), 610-618, (2015).
15. Satue, M. *et al.* Relationship between Visual Dysfunction and Retinal Changes in Patients with Multiple Sclerosis. *PLoS One*. **11** (6), e0157293, (2016).
16. Thomson, K.L., Yeo, J.M., Waddell, B., Cameron, J.R., Pal, S. A systematic review and meta-analysis of retinal nerve fiber layer change in dementia, using optical coherence tomography. *Alzheimer's & Dementia*. **1** (2), 136-143, (2015).
17. Dietrich, M. *et al.* Early alpha-lipoic acid therapy protects from degeneration of the inner retinal layers and vision loss in an experimental autoimmune encephalomyelitis-optic neuritis model. *Journal of Neuroinflammation*. **15** (1), 71, (2018).
18. Knier, B. *et al.* Neutralizing IL-17 protects the optic nerve from autoimmune pathology and prevents retinal nerve fiber layer atrophy during experimental autoimmune encephalomyelitis. *Journal of Autoimmunity*. **56**, 34-44, (2014).
19. Augustin, M. *et al.* In Vivo Characterization of Spontaneous Retinal Neovascularization in the Mouse Eye by Multifunctional Optical Coherence Tomography. *Investigative Ophthalmology & Visual Science*. **59** (5), 2054-2068, (2018).
20. Tode, J. *et al.* Thermal Stimulation of the Retina Reduces Bruch's Membrane Thickness in Age Related Macular Degeneration Mouse Models. *Translational Vision Science & Technology*. **7** (3), 2, (2018).
21. Gabriele, M.L. *et al.* Optic nerve crush mice followed longitudinally with spectral domain optical coherence tomography. *Investigative Ophthalmology & Visual Science*. **52** (5), 2250-2254, (2011).
22. Carpenter, C.L., Kim, A.Y., Kashani, A.H. Normative Retinal Thicknesses in Common Animal Models of Eye Disease Using Spectral Domain Optical Coherence Tomography. *Advances in Experimental Medicine and Biology*. **1074**, 157-166, (2018).
23. Alam, N.M. *et al.* A mitochondrial therapeutic reverses visual decline in mouse models of diabetes. *Disease Models & Mechanisms*. **8** (7), 701-710, (2015).
24. Bricker-Anthony, C., Rex, T.S. Neurodegeneration and Vision Loss after Mild Blunt Trauma in the C57Bl/6 and DBA/2J Mouse. *PLoS One*. **10** (7), e0131921, (2015).
25. Segura, F. *et al.* Assessment of Visual and Chromatic Functions in a Rodent Model of Retinal Degeneration. *Investigative Ophthalmology & Visual Science*. **56** (11), 6275-6283, (2015).
26. Fischer, M.D. *et al.* Noninvasive, in vivo assessment of mouse retinal structure using optical coherence tomography. *PLoS One*. **4** (10), e7507, (2009).

27. Ward, M.E. *et al.* Individuals with progranulin haploinsufficiency exhibit features of neuronal ceroid lipofuscinosis. *Science Translational Medicine*. **9** (385), (2017).
28. Chauhan, B.C. *et al.* Longitudinal in vivo imaging of retinal ganglion cells and retinal thickness changes following optic nerve injury in mice. *PLoS One*. **7** (6), e40352, (2012).
29. Lidster, K. *et al.* Neuroprotection in a novel mouse model of multiple sclerosis. *PLoS One*. **8** (11), e79188, (2013).
30. Munguba, G.C. *et al.* Nerve fiber layer thinning lags retinal ganglion cell density following crush axonopathy. *Investigative Ophthalmology & Visual Science*. **55** (10), 6505-6513, (2014).
31. Kokona, D., Jovanovic, J., Ebnetter, A., Zinkernagel, M.S. In Vivo Imaging of Cx3cr1gfp/gfp Reporter Mice with Spectral-domain Optical Coherence Tomography and Scanning Laser Ophthalmoscopy. *Journal of Visualized Experiments*. (129), (2017).
32. Leung, C. K. S. *et al.* In vivo imaging of murine retinal ganglion cells. *Journal of Neuroscience Methods*. **168** (2), 475-478, (2008).
33. Dietrich, M. *et al.* Whole-body positional manipulators for ocular imaging of anaesthetised mice and rats: A do-it-yourself guide. *BMJ Open Ophthalmology*. **1** (1), e000008, (2017).
34. Cruz-Herranz, A. *et al.* The APOSTEL recommendations for reporting quantitative optical coherence tomography studies. *Neurology*. **86** (24), 2303-2309, (2016).
35. Tewarie, P. *et al.* The OSCAR-IB consensus criteria for retinal OCT quality assessment. *PLoS One*. **7** (4), e34823, (2012).
36. Fan, Q., Teo, Y.-Y., Saw, S.-M. Application of advanced statistics in ophthalmology. *Investigative Ophthalmology & Visual Science*. **52** (9), 6059-6065, (2011).
37. Prusky, G.T., Alam, N.M., Beekman, S., Douglas, R.M. Rapid quantification of adult and developing mouse spatial vision using a virtual optomotor system. *Investigative Ophthalmology & Visual Science*. **45** (12), 4611-4616, (2004).
38. Groh, J., Stadler, D., Buttman, M., Martini, R. Non-invasive assessment of retinal alterations in mouse models of infantile and juvenile neuronal ceroid lipofuscinosis by spectral domain optical coherence tomography. *Acta Neuropathologica Communications*. **2**, 54, (2014).
39. Seeliger, M.W. *et al.* In vivo confocal imaging of the retina in animal models using scanning laser ophthalmoscopy. *Vision Research*. **45** (28), 3512-3519, (2005).
40. Shindler, K.S., Guan, Y., Ventura, E., Bennett, J., Rostami, A. Retinal ganglion cell loss induced by acute optic neuritis in a relapsing model of multiple sclerosis. *Multiple Sclerosis Journal*. **12** (5), 526-532 (2006).
41. Calderone, L., Grimes, P., Shalev, M. Acute reversible cataract induced by xylazine and by ketamine-xylazine anesthesia in rats and mice. *Experimental Eye Research*. **42** (4), 331-337 (1986).
42. Szczesny, G., Veihelmann, A., Massberg, S., Nolte, D., Messmer, K. Long-term anaesthesia using inhalatory isoflurane in different strains of mice—the haemodynamic effects. *Zeitschrift für mikroskopisch-anatomische Forschung*. **38** (1), 64-69, (2004).
43. Prusky, G.T., Harker, K., Douglas, R.M., Whishaw, I.Q. Variation in visual acuity within pigmented, and between pigmented and albino rat strains. *Behavioural Brain Research*. **136** (2), 339-348, (2002).
44. Wong, A.A., Brown, R.E. Visual detection, pattern discrimination and visual acuity in 14 strains of mice. *Genes, Brain, and Behavior*. **5** (5), 389-403, (2006).